Eur Biophys J (2012) 41:319–327
DOI 10.1007/s00249-012-0787-7

ORIGINAL PAPER

Biophysics in Europe

Extracellular electrical signals in a neuron-surface junction: model of heterogeneous membrane conductivity

Pavel M. Bulai · Pavel G. Molchanov · Andrey A. Denisov · Taras N. Pitlik · Sergey N. Cherenkevich

Received: 29 April 2009 / Revised: 23 December 2011 / Accepted: 12 January 2012 / Published online: 12 February 2012

Abstract Signals recorded from neurons with extracellular planar sensors have a wide range of waveforms and amplitudes. This variety is a result of different physical conditions affecting the ion currents through a cellular membrane. The transmembrane currents are often considered by macroscopic membrane models as essentially a homogeneous process. However, this assumption is doubtful, since ions move through ion channels, which are scattered within the membrane. Accounting for this fact, the present work proposes a theoretical model of heterogeneous membrane conductivity. The model is based on the hypothesis that both potential and charge are distributed homogeneously on the membrane surface, concentrated near channel pores, as the direct consequence of the inhomogeneous transmembrane current. A system of continuity equations having non-stationary and quasi-stationary forms expresses this fact mathematically. The present work performs mathematical analysis of the proposed equations, following by the synthesis of the equivalent electric element of a heterogeneous membrane current. This element is further used to construct a model of the cell-surface electric junction in a form of the equivalent electrical circuit. After that a study of how the heterogeneous membrane conductivity affects parameters of the extracellular electrical signal is performed. As the result it was found that variation of the passive characteristics of the cell-surface junction like conductivity of the cleft and the cleft height could lead to different shapes of the extracellular signals.

Keywords Neuron · Extracellular electrical signals · Cell-surface junction · Transmembrane current · Transchannel current · Heterogeneous membrane conductivity · Point-contact model

Introduction

Techniques of extracellular electrical recording and stimulation have made significant progress since the introduction of the first planar microelectrode arrays and field-effected transistors (Thomas et al. 1972; Bergveld et al. 1976; Gross et al. 1977) (Fig. 1). Microelectrode arrays fabricated according to modern semiconductor technologies often integrate multiple elements of passive and active circuitry. Arrays are used to effectively record, amplify and condition extracellular signals as well to perform extracellular stimulation (Eversmann et al. 2003; Lambacher et al. 2004). Nowadays microelectrode arrays are considered a basic platform for the development of cell-based sensors (Parce et al. 1989; DeBusschere and Kovacs 2001; Yeung et al. 2001; Pancrazio et al. 2003).

The application of microelectrode arrays gave a start to the long-term investigation of different dynamic processes taking place in cell cultures and tissue slices (Besl and Fromherz 2002; Heuschkel et al. 2002; Jimbo et al. 2006). A diversity of shapes and a wide range of amplitudes of signals recorded with planar electrodes from different neurons have been reported (Gross 1979; Regehr et al. 1989; Bove 1995; Breckenridge et al. 1995; Jenkner and Fromherz 1997; Schatzthauer and Fromherz 1998; Fromherz 1999; Ruardij et al. 2009). Signals were generally classified (arranged in types) according to the waveform and amplitude (Fromherz 2003). This classification is used conventionally for spike detection and sorting in the cell

P. M. Bulai (✉) · P. G. Molchanov · A. A. Denisov · T. N. Pitlik · S. N. Cherenkevich
Department of Biophysics, Physics Faculty, Belarusian State University, Nezavisimosty Av. 4, 220050 Minsk, Belarus
e-mail: bulaypm@bsu.by

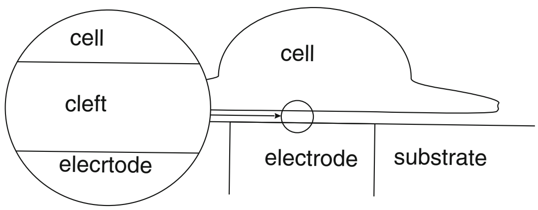

Fig. 1 Schematic view of an electrode covered with neurons

population (Salganicoff et al. 1988; Sarna et al. 1988) as well as for an individual cell characterization (Stett et al. 2003). In cited papers all signal types were explained as originating from and being simulated on the basis of several possible mechanisms: the asymmetry of the cell soma and neurite shapes (Bove et al. 1994; Gold et al. 2006), variability of sealing resistance in the neuron-electrode electrical contact (Grattarola and Martinoia 1993) and the membrane channel distributions (Jenkner and Fromherz 1997; Schatzthauer and Fromherz 1998; Fromherz 1999; Buitenweg et al. 2002).

Up to date main models for signal simulation are: current source field integration (Plonsey 1964; Plonsey and Barr 2007), equivalent electric circuits (Regehr et al. 1989; Grattarola and Martinoia 1993) and geometry-based finite-element modeling (Buitenweg et al. 2002; Heuschkel et al. 2002). In these models the membrane current is described with a stationary continuity equation. In the integrated form, the stationary continuity equation corresponds to Kirchhoff's law. According to Kirchhoff's law, the membrane current is a sum of capacitive and ionic currents:

$$j_m(\psi_m) = c_m \frac{\partial \Delta\psi_m}{\partial t} + j_c(\Delta\psi_m), \qquad (1)$$

where, j_m is the total membrane current density, ψ_m is a membrane potential, $\Delta\psi_m$ is a transmembrane potential, c_m is a membrane specific capacitance, t is the time variable, and j_c is the ionic current density.

It should be pointed out that Kirchhoff's law for the membrane current in Eq. 1 assumes the homogeneous flow of the charge through the membrane. However, on the biological basis, the transmembrane current is flowing through ion channels and not through the whole cellular membrane. The total channel cross-section area is less than 0.01% of the total membrane area (Nicholls et al. 2001). In addition, the distance between channels of identical types often can be even larger than the distance between the cellular membrane and the sensor surface (the distance between channels can be estimated from the conductivity of the membrane and the channels).

In the case of a homogeneous charge flow in Eq. 1, the value of the transmembrane current is the function of the membrane conductivity only. However, if the charge is transferred through the membrane channels, then the conductivity of solution near the membrane should directly influence the charge relaxation on membrane surfaces and, consequently, the total membrane current (Fig. 2).

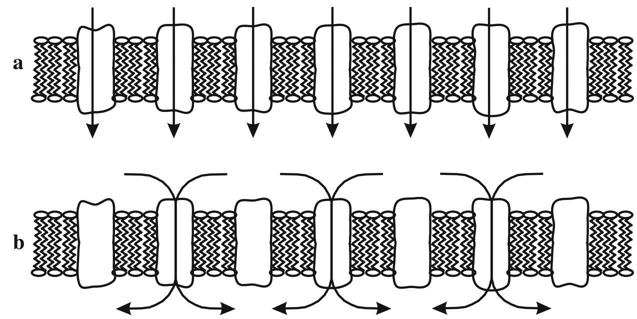

Fig. 2 Difference between homogenous (**a**) and heterogeneous (**b**) membrane conductivity

The present work proposes a theoretical model of heterogeneous membrane conductivity. The model is based on the hypothesis that the electrical potential as well as charge is distributed homogeneously on membrane surfaces because of the transmembrane current inhomogeneity. The model is expressed with a system of continuity equations and has non-stationary and quasi-stationary forms.

To obtain parameters for the heterogeneous membrane conductivity model, a charge flow through the single membrane pore (channel) was computationally simulated. The potential-to-charge ratio in the vicinity of the membrane channel was estimated as a function of the membrane capacitance, channel radius and average channel density empirically.

In the next step the equivalent electric element of the cellular membrane was developed. It was based on the heterogeneous membrane conductivity model, which implies that the membrane conductivity of the element has dependence on the medium conductivity on both sides of the membrane.

This equivalent electric element of the heterogeneous membrane current was further employed in a model of the cell-surface electric junction. Built in the form of the equivalent electrical circuit, the model was used to evaluate effects of heterogeneity in membrane conductivity on signal parameters. The main types of extracellular electrical signals have been acquired when this model was subjected to various cell-surface junction heights and junction conductivities.

Model of heterogeneous membrane conductivity

When the charge is traveling in and out of the channel pore, it creates the region of excess charge Q_e and overpotential ψ_e just near the end of the channel. The values of the additional excess charge Q_e and overpotential ψ_e can be conveniently

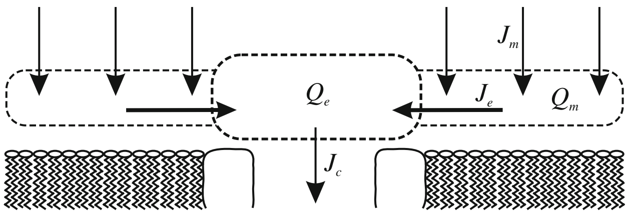

Fig. 3 Scheme of the heterogeneous membrane conductivity model: relative positions of the excess Q_e and homogeneous Q_m charges, directions of the channel J_c, lateral J_e and total membrane J_m currents

defined in relation to a spatially homogeneous charge Q_m and potential ψ_m on the rest of the membrane surface. The existence of the overpotential near the pore allows defining a transchannel potential (total local potential over the channel) as the sum of $\Delta\psi_m + \Delta\psi_e$, which is obviously different from the simple transmembrane potential $\Delta\psi_m$ and which actually should be used when one calculates the conductance of the potential-dependent channel.

Following this, a general scheme of the model can be described as a two-step process: charge transfer into the region with the excess charge near the end of the membrane channel followed by the immediate drifting of the transferred charge into the spatially homogeneous charge region nearby (Fig. 3).

The rate of change of the excess charge Q_e is the sum of the current through the channel J_c and a lateral relaxation current J_e as depicted in Fig. 3. At the same time the rate of change of the spatially homogeneous charge Q_m is equal to the sum of the lateral relaxation current J_e and a transmembrane current J_m (the charge migration current). These statements can be written as:

$$\begin{cases} \frac{\partial Q_m}{\partial t} = -J_e + J_m, \\ \frac{\partial Q_e}{\partial t} = J_e - J_c. \end{cases} \quad (2)$$

In the system of Eq. 2 the value of the lateral relaxation current J_e is the total current flowing inward through an imaginary closed surface covering the excess charge Q_e region. Applying Ohm's law and the Gauss-Ostrogradsky theorem to Gauss's law, the following equation can be derived:

$$J_e = -\frac{\delta}{\varepsilon} Q_e, \quad (3)$$

where δ is the conductivity of a solution and ε is the dielectric permittivity of the solution.

Since the value of the current through the channel J_c now is a function of the total potential $\Delta\psi_m + \Delta\psi_e$ and the value of the transmembrane current is a function of the spatially homogeneous potential ψ_m, the system of Eq. 2 may be rewritten in the next form:

$$\begin{cases} \frac{\partial Q_m}{\partial t} = \frac{\delta}{\varepsilon} Q_e + J_m(\psi_m), \\ \frac{\partial Q_e}{\partial t} = -\frac{\delta}{\varepsilon} Q_e - J_c(\Delta\psi_m + \Delta\psi_e). \end{cases} \quad (4)$$

In the system of Eq. 4, values of homogeneous and excess charges relate to the homogeneous potential and overpotential accordingly:

$$\begin{aligned} Q_m &= C_m \Delta\psi_m, \\ Q_e &= C_m K_e \psi_e. \end{aligned} \quad (5)$$

where K_e is a coefficient that connects values of the excess charge and overpotential near the channel end. K_e will be discussed and estimated later.

Substitution of Eq. 5 into Eq. 4 gives a non-stationary form of the heterogeneous membrane conductivity model:

$$\begin{cases} C_m \frac{\partial \Delta\psi_m}{\partial t} = \frac{\delta}{\varepsilon} C_m K_e \psi_e + J_m(\psi_m), \\ C_m K_e \frac{\partial \psi_e}{\partial t} = -\frac{\delta}{\varepsilon} C_m K_e \psi_e - J_c(\Delta\psi_m + \Delta\psi_e). \end{cases} \quad (6)$$

In the second equation of Eq. 6 the ratio $\varepsilon/\delta = \tau$ is a time constant, which defines a rate of the excess charge relaxation. In the case of physiological saline estimation gives $\tau \approx 10^{-9}$ s. It is much less than the channel activation time. As a result one may conclude that the excess charge reaches a stationary value much faster than the homogeneous charge and transmembrane potential do. With this condition met the second differential equation can be replaced by the algebraic Eq. 7.

$$\begin{cases} C_m \frac{\partial \Delta\psi_m}{\partial t} = \frac{\delta}{\varepsilon} C_m K_e \psi_e + J_m(\psi_m), \\ 0 = -\frac{\delta}{\varepsilon} C_m K_e \psi_e - J_c(\Delta\psi_m + \Delta\psi_e). \end{cases} \quad (7)$$

In the system of Eq. 7 performing addition of the second equation to the first one leads to the equation (first in Eq. 8) in a form similar to Eq. 1. The value of the overpotential ψ_e could be derived from the second equation in Eq. 7. The system of Eq. 8 is a quasi-stationary form of the heterogeneous membrane conductivity model.

$$\begin{cases} C_m \frac{\partial \Delta\psi_m}{\partial t} = -J_c(\Delta\psi_m + \Delta\psi_e) + J_m(\psi_m), \\ \psi_e = -\frac{\varepsilon}{\delta} \frac{J_c(\Delta\psi_m + \Delta\psi_e)}{C_m K_e}. \end{cases} \quad (8)$$

It can be seen from the second equation in Eq. 8 that the smaller conductivity of the environment near the channels pore is, the greater the overpotential might appear.

Homogeneous membrane conductivity (Eq. 1) is a special case of a model of heterogeneous membrane conductivity (Eq. 8): the value of overpotential ψ_e becomes insignificant under the conditions that the conductivity of solution δ and factor K_e are big and/or the transchannel current J_c is small.

Channel density factor

The coefficient K_e that binds values of the excess charge and overpotential near the channel was introduced in the second equation of Eq. 5. This coefficient has a natural dependence both on the channel as well as on patch geometry and dimensions, making it hard to describe analytically in general. However, numerical computational simulations of the ion current flowing through the membrane pore (channel) provide a convenient means to obtain this coefficient at least for a specific case.

The geometry that was used in simulations represents a cylinder separated into two halves with a membrane containing a single pore. The cylinder has a height equal to 400 nm and a radius $r_m = 200$ nm. The thickness of the membrane is 10 nm, and the radius of the pore is $r_c = 0$–200 nm. The whole geometry has an axial symmetry. The compartment and channel are considered to be filled with the 0.1 M binary aqueous electrolyte (KCl) at 300 K. A relative permittivity of the membrane is equal to 4.

The transient drift–diffusion (Nernst-Planck-Poisson) problem was used to describe the spatio-temporal distribution of potential and charge within the system. Boundary conditions for concentrations are considered the insulation barrier at the compartment and membrane surfaces. Boundary conditions that are related to the potential distribution were: absence of any charges on the side, top and bottom surfaces of the geometry, continuity of the electric potential on the membrane and pore boundaries. Potential at a point in the middle of the membrane at the compartment side was taken to be a zero reference potential.

The drift–diffusion problem was solved with the finite-element method using a program environment of COMSOL Multiphysics (COMSOL Group). The application modes were chosen to be the "Nernst-Planck without Electroneutrality" and "Electrostatic." The space dimension had 2D axial symmetry. A non-uniform grid with a higher density near the membrane (element size 1 nm) and pore (element size 0.1 nm) was used. Computations were performed with the BDE time dependent solver and direct (UMFPACK) linear system solver.

To set up the initial conditions the membrane was allowed to be charged by applying the step of the transmembrane potential of 100 mV. The transmembrane potential was applied by setting a fixed potential on the top and bottom of the geometry compartments. At the appropriate time after this, the spatially homogeneous charge appeared near the membrane. After the charging, the top and bottom boundaries of the compartment were set to have a zero charge, and the membrane started a slow discharge process by ions drifting through the pore. During the drifting phase the electric potential and surface charge density at the plane of the membrane side were observed. The surface charge density was obtained by integration of a spatial charge density in the direction orthogonal to the membrane. The simulation was performed for a set of different radii of the pore: from 0 to 200 nm.

Results of the simulation for the channel radius $r_c = 5$ nm at an arbitrary selected time (as an example) are shown in Fig. 4. Corresponding profiles of the potential and surface charge density on the membrane/channel surface are presented in Fig. 5.

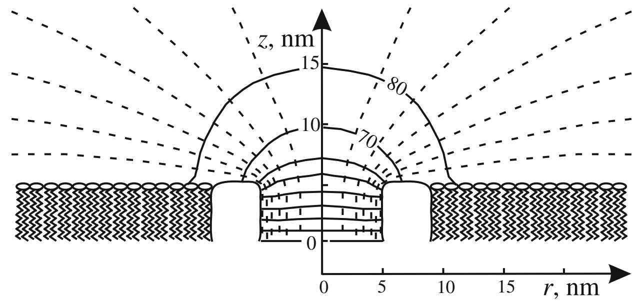

Fig. 4 Results of the solution for the mixed Nernst-Planck-Poisson problem in cylindrical coordinates (z, r) for the channel of radius $r_c = 5$ nm in an arbitrary point of time: equipotential surfaces and current lines

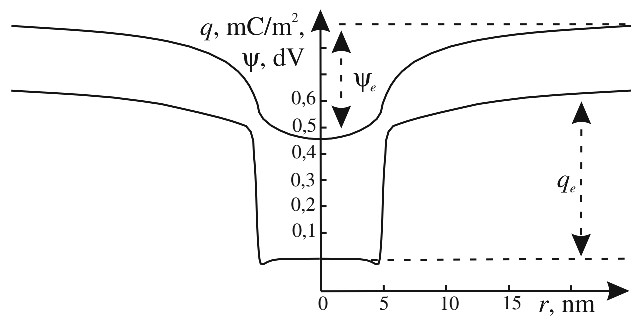

Fig. 5 Results of the solution for the mixed Nernst-Planck-Poisson problem in cylindrical coordinates (z, r) for the channel of radius $r_c = 5$ nm in an arbitrary point of time: profiles of the potential and surface charge density on the membrane/channel surface

Excess charge density q_e and overpotential ψ_e were obtained in the point that laid on the channel axis just near the channel end. From simulations for different channel radii, the relationship between q_e and ψ_e was found to be independent on the channel current, but it did depend on the channel and patch radii (Fig. 6). This relationship appeared to be well approximated by the curve given by Eq. 9, where λ is the Debye length:

$$\frac{q_e}{\psi_e} = c_m \frac{4\lambda + r_c}{r_c} \frac{2r_m - r_c}{r_m - r_c}. \tag{9}$$

The K_e function is expressed by Eqs. 5 and 9, using $Q_e = \pi r_c^2 q_e$ and $C_m = \pi r_m^2 c_m$, to get the following formula:

$$K_e = \frac{r_c^2}{r_m^2} \frac{4\lambda + r_c}{r_c} \frac{2r_m - r_c}{r_m - r_c}. \tag{10}$$

Equation 10 can be further simplified in the case when: $r_m \gg r_c$—which means a low channel density—and $r_c \approx \lambda$—which means that a minimal size of a screened charge in the solution is equal to the Debye length. By applying these assumptions, one can express:

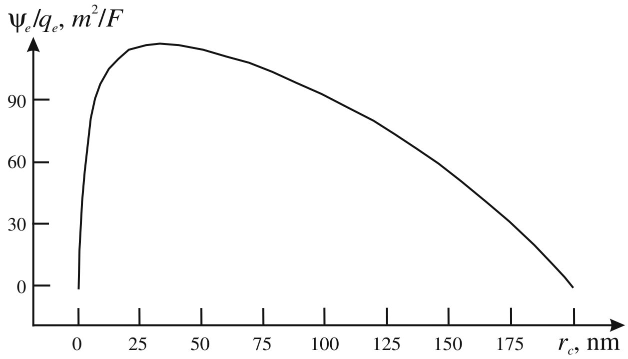

Fig. 6 Results of the solution for the mixed Nernst-Planck-Poisson problem for different channel radii: relationship between the excess charge density q_e and overpotential ψ_e in the dependence on channel radius

$$K_e = 10\frac{\lambda^2}{r_m^2}. \quad (11)$$

After introduction of the ion channel density $\eta = 1/\pi r_m^2$, Eq. 11 can be rewritten as:

$$K_e = 10\pi\eta\lambda^2. \quad (12)$$

Thus, the K_e function can be called a channel density factor.

Equivalent electric element of heterogeneous membrane current

Equations of the heterogeneous membrane conductivity model could be modified into the equivalent electric element of membrane current that can be used in the cell-surface junction point contact model.

The non-stationary form of the heterogeneous membrane conductivity model in Eq. 6 can be rewritten in the form of the following Eqs. 13 and 14:

$$J_m(\psi_m) = C_m\frac{\partial\Delta\psi_m}{\partial t} + J_e(\psi_m), \quad (13)$$

where:

$$\begin{cases} J_e(\psi_m) = -\frac{\delta}{\varepsilon}C_m K_e\psi_e, \\ \frac{\partial\psi_e}{\partial t} = -\frac{\delta}{\varepsilon}\psi_e - \frac{J_c(\Delta\psi_m+\Delta\psi_e)}{C_m K_e}. \end{cases} \quad (14)$$

The system of Eq. 14 could be rewritten in terms of the capacitance and current surface density:

$$\begin{cases} j_e(\psi_m) = -\frac{\delta}{\varepsilon}c_m K_e\psi_e, \\ \frac{\partial\psi_e}{\partial t} = -\frac{\delta}{\varepsilon}\psi_e - \frac{j_c(\Delta\psi_m+\Delta\psi_e)}{c_m K_e}. \end{cases} \quad (15)$$

The system of Eq. 15 describes the current density only at one side of the membrane. To complete the membrane description with a second side all equations in the system of Eq. 15 were doubled for the inner (in) and outer (out) current densities:

$$\begin{cases} j_e^{in}(\psi_m^{in}) = -\frac{\delta^{in}}{\varepsilon}c_m K_e\psi_e^{in}, \quad j_e^{out}(\psi_m^{out}) = -\frac{\delta^{out}}{\varepsilon}c_m K_e\psi_e^{out}, \\ \frac{\partial\psi_e^{in}}{\partial t} = -\frac{\delta^{in}}{\varepsilon}\psi_e^{in} - \frac{j_c(\Delta\psi_m+\Delta\psi_e)}{c_m K_e}, \quad \frac{\partial\psi_e^{out}}{\partial t} = -\frac{\delta^{out}}{\varepsilon}\psi_e^{out} + \frac{j_c(\Delta\psi_m+\Delta\psi_e)}{c_m K_e}, \\ \Delta\psi_m = \psi_m^{in} - \psi_m^{out}, \\ \Delta\psi_e = \psi_e^{in} - \psi_e^{out}. \end{cases} \quad (16)$$

Finally, currents were written down for all type of ions, which in our case are Na, K and Cl:

$$\begin{cases} j_e^{in}(\psi_m^{in}) = -\frac{\delta^{in}}{\varepsilon}c_m\sum_n K_e^n\psi_e^{n,in}, \quad j_e^{out}(\psi_m^{out}) = -\frac{\delta^{out}}{\varepsilon}c_m\sum_n K_e^n\psi_e^{n,out}, \\ \frac{\partial\psi_e^{n,in}}{\partial t} = -\frac{\delta^{in}}{\varepsilon}\psi_e^{n,in} - \frac{j_c^n(\Delta\psi_m+\Delta\psi_e^n)}{c_m K_e^n}, \quad \frac{\partial\psi_e^{n,out}}{\partial t} = -\frac{\delta^{out}}{\varepsilon}\psi_e^{n,out} + \frac{j_c^n(\Delta\psi_m+\Delta\psi_e^n)}{c_m K_e^n}, \\ \Delta\psi_m = \psi_m^{in} - \psi_m^{out}, \\ \Delta\psi_e^n = \psi_e^{n,in} - \psi_e^{n,out}, \\ n = \mathrm{Na, K, Cl}. \end{cases} \quad (17)$$

By analogy with Eqs. 14–17 the quasi-stationary form of the equivalent electric element takes the next form:

$$\begin{cases} j_e^{in}(\psi_m^{in}) = -j_e^{out}(\psi_m^{out}) = \sum_n j_c^n(\Delta\psi_m + \Delta\psi_e^n), \\ \psi_e^{n,in} = -\frac{\delta^{out}}{\delta^{in}}\psi_e^{n,out} = -\frac{\varepsilon}{\delta^{in}}\frac{j_c^n(\Delta\psi_m+\Delta\psi_e^n)}{c_m K_e^n}, \\ \Delta\psi_m = \psi_m^{in} - \psi_m^{out}, \\ \Delta\psi_e^n = \psi_e^{n,in} - \psi_e^{n,out}, \\ n = \mathrm{Na, K, Cl}. \end{cases} \quad (18)$$

Thus, Eq. 17 is the non-stationary form, and Eq. 18 is the quasi-stationary form of the equivalent electric element of the membrane heterogeneous current. The electrical current in the equivalent element depends on the transmembrane potential as well as on intra- and extracellular conductivities of the solution.

Cell-surface junction point-contact model

The main interest, which remains till this point, is to figure out how the heterogeneous membrane conductivity could affect the shape of the recordable extracellular signal under various conditions. One approach could be the development of a simplified point-contact cell-surface junction model describing the extracellular electrical arrangement between the cell and the sensor.

A sufficiently simplified point-contact model that could describe the experiment may include five compartments as referred to in Fig. 7: a cell (c), an external solution (s), a junction between a cell and a surface (j), a measuring electrode (l) and, finally, a reference electrode (r).

Now in order to describe a cellular membrane the equivalent electric element of the heterogeneous membrane current should be used. The non-stationary form of the equivalent electric element was exploited because of the fact that a numerical solution of Eq. 17 is more stable. Ion

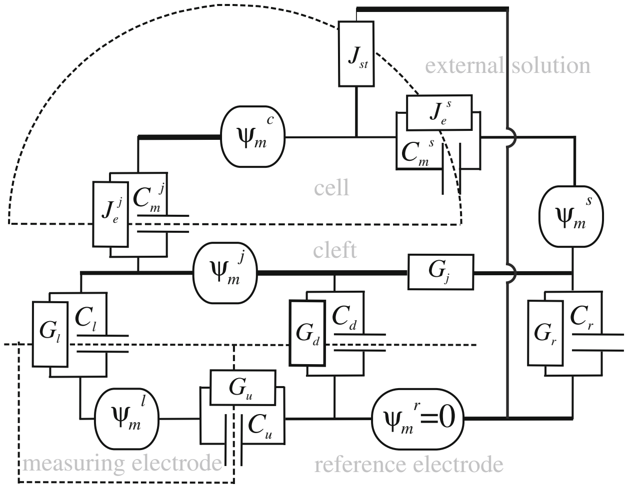

Fig. 7 Equivalent circuit of the cell-surface junction point-contact model (list of symbols in Table 1)

currents through channels j_c^n were introduced by a set of Hodgkin-Huxley equations (Hodgkin and Huxley 1952).

The Ohm's law was applied to calculate currents through other homogeneous borders. Values of parameters and sizes of boundaries are summarized in the Table 1. To calculate the seal conductance of the cleft the following formula was used (Fromherz 2003):

$$G_j = 4\pi\delta_j h, \quad (19)$$

where δ_j is the conductivity of the cleft, and h is the cleft height.

Additional transmembrane current (0.3 nA) was injected into the cell to stimulate electrical activity.

The equivalent circuit of the model corresponds to the initial value problem for a first-order differential equation system. Matlab software (MathWorks) multistep solver *ode*15 s based on variable-order numerical differentiation formulas was used to solve the problem.

Results and discussion

Parameters, which determine a type of cell-surface junction, are the conductivity of the cleft (δ_j) and the cleft height (h). Both determine the seal conductance of the cleft according to the Eq. 19. At the same time, the conductivity of the cleft determines the value of the excess charge and overpotential near the membrane channels according to Eqs. 4, 6. As a consequence, the conductivity of the cleft influences the potential drop that appears across the channel, which in turn controls the channel current.

A decrease in the conductivity of the cleft results in excess charge build up and overpotential increase near the channel pore. For sodium channels the excess charge and

Table 1 Parameters of the cell-surface junction point-contact model

Variables and parameters	Symbol	Value
Intracellular potential	ψ_m^c	
Potential in the cleft	ψ_m^j	
Potential of the measuring electrode	ψ_m^l	
Potential in an external solution	ψ_m^s	
Potential of a reference electrode	ψ_m^r	0 mV
Dielectric permittivity of the solution	ε	$81{\cdot}\varepsilon_0$ F/m
Debye length	λ	1 nm
Cleft height	h	5–105 nm
Conductivity of the cleft	δ_j	0.06–1.80 S/m
Conductivity of the external solution	δ_s	1.8 S/m
Conductivity of the cell	δ_c	0.6 S/m
Total membrane current of a bottom cell patch	J_e^s	$j_e^s \cdot S_m^s$
Total membrane current of a top cell patch	J_e^j	$j_e^j \cdot S_m^j$
Capacitance of the top cell patch	C_m^s	$c_m \cdot S_m^s$
Capacitance of the bottom cell patch	C_m^j	$c_m \cdot S_m^j$
Capacitance of the measuring electrode	C_l	$c_l{\cdot}S_l$
Capacitance of the reference electrode	C_r	$c_r{\cdot}S_r$
Capacitance of the measuring electrode in substrate	C_u	$c_u{\cdot}S_u$
Capacitance of the substrate	C_d	$c_d{\cdot}S_d$
Conductance of the measuring electrode	G_e	$g_e{\cdot}S_e$
Conductance of the reference electrode	G_r	$g_r{\cdot}S_r$
Conductance of the measuring electrode in substrate	G_u	$g_u{\cdot}S_u$
Conductance of the substrate	G_d	$g_d{\cdot}S_d$
Specific capacitance of the membrane	c_m	50 mF/m^2
Specific capacitance of the measuring electrode	c_e	2 mF/m^2
Specific capacitance of the reference electrode	c_r	2 mF/m^2
Specific capacitance of the measuring electrode in substrate	c_u	1 mF/m^2
Specific capacitance of the substrate	c_d	3 mF/m^2
Conductivity of the measuring electrode	g_e	1 S/m^2
Conductivity of the reference electrode	g_r	1 S/m^2
Conductivity of the measuring electrode in substrate	g_u	1 mS/m^2
Conductivity of the substrate	g_d	1 mS/m^2
Area of the top cell patch	S_m^s	2,000 μm^2
Area of the bottom cell patch	S_m^j	1,000 μm^2
Area of the measuring electrode	S_l	300 μm^2
Area of the reference electrode	S_r	1,000 mm^2
Area of the measuring electrode in substrate	S_u	300 μm^2
Area of the substrate	S_d	700 μm^2
Channel density factor for sodium channels	K_e^{Na}	1×10^5
Channel density factor for potassium channels	K_e^{K}	3×10^5
Channel density factor for chlorine channels	K_e^{Cl}	2×10^6

overpotential in the cleft have negative values. This leads to a more rapid transchannel potential depolarization (here more rapid means when compared with the membrane depolarization) and results in the early sodium channel activation. On the contrary, for potassium channels, the excess charge and overpotential in the cleft have positive values. This lowers the transchannel potential depolarization (when compared with the membrane depolarization) and reduces the potassium channel current (Fig. 8). A further decrease of the conductivity brings the potential difference over the channel down and leads to a further current recession. This effect is similar to a channel closure. As result, the less the conductivity of the cleft is, the more rapidly the sodium current increases and less of the potassium current flows (Fig. 8).

Extracellular electrical signals simulated for different values of the conductivity of the cleft and the cleft height are shown in the Fig. 9.

Because of the low conductance of the measuring electrode G_u, its potential ψ_m^l is equal to the potential in the cleft ψ_m^j. This electrical potential is controlled by Kirchhoff's law, which takes the next form:

$$C_d \frac{\partial\left(\psi_m^j - \psi_m^r\right)}{\partial t} + \psi_m^j G_j = C_m^j \frac{\partial\left(\psi_m^c - \psi_m^j\right)}{\partial t} + J_e^j\left(\delta_j, J_c^j\right) \quad (20)$$

When conductivity of the cleft is large, for example, equal to the conductivity of the extracellular solution, overpotential near the channels on the bottom and top membrane halves is small and equal among themselves. This situation is the symmetrical charge transfer process, when ionic and capacitive currents have similar magnitudes but opposite directions. As a result the total membrane current vanishes, and the extracellular potential has a small amplitude (A-type signals on Figs. 9, 10).

Under conditions when the conductivity of the cleft is moderate and the capacitance of the substrate is small, the cleft signal shape is proportional to the total membrane current, and the signal amplitude depends on the seal conductance (Eq. 20). This type of contact can be called "ohmic". The total membrane current now is the sum of the current through the membrane capacitance with ionic currents through channels (Eq. 20). A more rapid sodium current increase leads to a more apparent first negative peak in the extracellular signal shape (C, D-type signals in Figs. 9, 10).

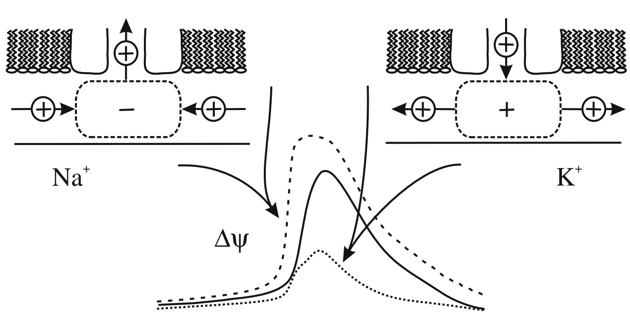

Fig. 8 Shifts in the transchannel potential waveform for sodium (*dashed lines*) and potassium (*dotted lines*) channels relative to the transmembrane potential (*solid lines*) with the low conductivity in the cleft

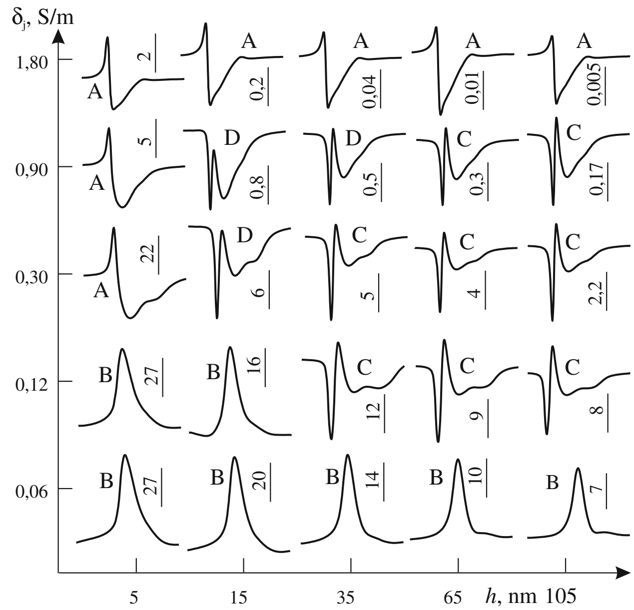

Fig. 9 Dependence of extracellular signal amplitudes (amplitude in mV, signal duration is 15 ms) and shapes (*A*, *B*, *C*, *D*-type) on the cleft height and on the conductivity of the cleft

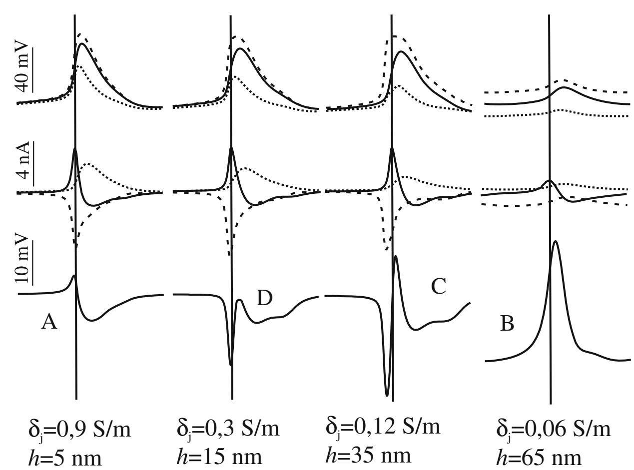

Fig. 10 Main types of extracellular electrical signals (in the *third row*) and corresponding to them: transchannel (*dashed lines* Na, *dotted lines* K) and transmembrane (*solid lines*) potentials (in the *first row*), currents (*dashed lines* Na, *dotted lines* K, *solid lines* capacitive) (in the *second row*), the lateral conductivity and the cleft height (in the *fourth row*)

In the situation when the conductivity of the cleft is very small, say approximately 30 times less than the conductivity of the extracellular solution, the seal conductance as well as the potential difference across the channel is considerably small. If this potential falls below an excitation threshold, ionic channels of the bottom cellular membrane may not be activated. In this case the extracellular signal ψ_m^j is proportional to the intracellular potential ψ_m^c, and the amplitude of the signal depends on the membrane and substrate capacitances (Eq. 20). This type of contact can be called "capacitive". For this contact type, the amplitude of the extracellular signal increases because of the decrease in the seal conductance (B-type signals in Figs. 9, 10).

It is interesting to note that all signals in Fig. 9 were obtained with the same value of the seal conductance of the cleft $\sim$54 nS (according to the Eq. 10), which corresponds to the seal resistance value of 18.5 MOhm.

Signals with shapes corresponding to the main types (A-, B-, C-, D-type) of extracellular signals, which were found experimentally and described by other authors (Jenkner and Fromherz 1997; Schatzthauer and Fromherz 1998; Fromherz 1999), could be seen among simulated extracellular signals (Figs. 9, 10). Shapes of other signals represent a combination of these basic types of signals.

Conclusion

With the aid of the heterogeneous membrane conductivity model, it was shown that changes in the passive cell-surface junction characteristics (like the conductivity of the cleft and the cleft height) may appear to be a sufficient cause of different types of extracellular signals.

Without any doubt the proposed heterogeneous membrane conductivity model describes only one of the possible mechanisms of extracellular signal formation. The heterogeneous membrane conductivity mechanism was tested alone to show its applicability in the presented point-contact model of the cell-surface junction. To describe or simulate a full realistic picture of the signal formation process, one has to take into consideration all possible mechanisms mentioned in the introduction.

The effects of the heterogeneous membrane conductivity will be significant if signals are registered in close cell-electrode contact. If the cells are far away from the electrode, then the relative position of the cell soma and neurites will determine the signal shape (Gold et al. 2006).

The point-contact model was used to simulate signal recording from a current-stimulated cell. Cell stimulation can also be simulated by applying a constant or variable electric potential in one of the nodes $\left(\psi_m^c\ \psi_m^j\ \psi_m^l\ \psi_m^s\right)$ of the equivalent circuit of the cell-surface junction (Fig. 7).

The heterogeneous membrane conductivity model is heavily based on continuum electrostatics to describe the charge and potential near the membrane channel. Of course, at the nanometer level Brownian and molecular dynamics methods could be preferred over the Nernst-Planck-Poisson method (Corry et al. 2000). But the Nernst-Planck-Poisson theory is very useful for the ensemble-averaged description.

Hodgkin-Huxley equations, which were used to describe currents through channels (Hodgkin and Huxley 1952), could be altered to reflect other sorts of ion channels with the current kinetics different for various types of cells. However, as a result, extracellular signal shapes could be changed to some extent.

The cleft height in the average cell-surface junction was reported to be 50–70 nm (Fromherz 2003). A wider range of the cleft heights was intentionally used in the simulation to demonstrate the signal waveform and amplitude dependence on the height.

It is also necessary to note that the conductivity of the cleft together with the cleft height unambiguously determines the electric properties of the cell-surface junction. Therefore, they can be used as the characteristic properties of the cellular adhesion to various surfaces.

References

Bergveld P, Wiersma J, Meertens H (1976) Extracellular potential recordings by means of a field effect transistor without gate metal called OSFET. IEEE Trans Biomed Eng 23:136–144

Besl B, Fromherz P (2002) Transistor array with an organotypic brain slice: field potential records and synaptic currents. Eur J Neurosci 15:999–1005

Bove M, Grattarola M, Martinoia S, Verreschi G (1995) Interfacing cultured neurons to planar substrate microelectrodes: characterization of the neuron-to-microelectrode junction. Bioelectrochem Bioenerg 38:255–265

Bove M, Massobrio G, Martinoia S, Grattarola M (1994) Realistic simulations of neurons by means of an ad hoc modified version of SPICE. Biol Cybern 71:137–145

Breckenridge LJ, Wilson RJA, Connolly P, Curtis ASG, Dow JAT, Blackshaw SE, Wilkinson CDW (1995) Advantages of using microfabricated extracellular electrodes for in vitro neuronal recording. J Neurosci Res 42:266–276

Buitenweg JR, Rutten WL, Marani E (2002) Modeled channel distributions explain extracellular recordings from cultured neurons sealed to microelectrodes. IEEE Trans Biomed Eng 49:1580–1590

Corry B, Kuyucak S, Chung SH (2000) Tests of continuum theories as models of ion channels. II. Poisson-Nernst-Planck theory versus brownian dynamics. Biophys J 78:2364–2381

DeBusschere BD, Kovacs GTA (2001) Portable cell-based biosensor system using integrated CMOS cell-cartridges. Biosens Bioelectron 16:543–556

Eversmann B, Jenkner M, Hofmann F, Paulus C, Brederlow R, Holzapfl B, Fromherz P, Merz M, Brenner M, Schreiter M, Gabl R, Plehnert K, Steinhauser M, Eckstein G, Schmitt-Landsiedel

D, Thewes R (2003) A 128 × 128 CMOS biosensor array for extracellular recording of neural activity. IEEE J Solid-State Circuits 38:2306–2317

Fromherz P (1999) Extracellular recording with transistors and the distribution of ionic conductances in a cell membrane. Eur Biophys J 28:254–258

Fromherz P (2003) Neuroelectronic interfacing: semiconductor chips with ion channels, nerve cells and brain. In: Waser R (ed) Nanoelectronics and information technology. Wiley-VCH, Berlin, pp 781–810

Gold C, Henze DA, Koch C, Buzsaki G (2006) On the Origin of the extracellular action potential waveform: a modeling study. J Neurophysiol 95:3113–3128

Grattarola M, Martinoia S (1993) Modeling the neuron-microtransducer junction: from extracellular to patch recording. IEEE Trans Biomed Eng 40:35–41

Gross GW (1979) Simultaneous single unit recording in vitro with a photoetched laser deinsulated gold multi-microelectrode surface. IEEE Trans Biomed Eng 26:273–279

Gross GW, Rieske E, Kreutzberg GW, Meyer A (1977) A new fixed-array multi-microelectrode system designed for long-term monitoring of extracellular single unit neuronal activity in vitro. Neurosci Lett 6:101–105

Heuschkel M, Fejtl M, Raggenbass M, Bertrand D, Renaud P (2002) A three-dimensional multi-electrode array for multi-site stimulation and recording in acute brain slices. J Neurosci Methods 114:135–148

Hodgkin AL, Huxley AF (1952) A quantitave description of membrane current and its application to conduction and excitation in nerve. J Physiol 117:500–544

Jenkner M, Fromherz P (1997) Bistability of membrane conductance in cell adhesion observed in a neuron transistor. Phys Rev Lett 79:4705–4708

Jimbo Y, Kasai N, Torimitsu K, Tateno T (2006) MEA-based spike recording in cultured neuronal networks. In: Xing W-L, Cheng J (eds) Frontiers in biochip technology. Springer, US, pp 88–98

Lambacher A, Jenkner M, Merz M, Eversmann B, Kaul RA, Hofmann F, Thewes R, Fromherz P (2004) Electrical imaging of neuronal activity by multi-transistor-array (MTA) recording at 7.8 μm resolution. Appl Phys A 79:1607–1611

Nicholls JG, Martin AR, Wallace BG, Fuchs PA (2001) From neuron to brain. Sinauer Associates, Inc., Sunderland

Pancrazio JJ, Gray SA, Shubin YS, Kulagina N, Cuttino DS, Shaffer KM, Eisemann K, Curran A, Zim B, Gross GW, O'Shaughnessy TJ (2003) A portable microelectrode array recording system incorporating cultured neuronal networks for neurotoxin detection. Biosens Bioelectron 18:1339–1347

Parce JW, Owicki JC, Kercso KM, Sigal GB, Wada HG, Muir VC, Bousse LJ, Ross KL, Sikic BI, McConnell HM (1989) Detection of cell-affecting agents with a silicon biosensor. Science 246:243–247

Plonsey R (1964) Volume conductor fields of action currents. Biophys J 4:317–328

Plonsey R, Barr RC (2007) Extracellular fields. In: Bioelectricity: a quantitative approach. Springer, US, pp 223–265

Regehr WG, Pine J, Cohan CS, Mischke MD, Tank DW (1989) Sealing cultured invertebrate neurons to embedded dish electrodes facilitates long-term stimulation and recording. J Neurosci Methods 30:91–106

Ruardij TG, Rutten WLC, van Staveren G, Roelofsen BH (2009) Spontaneous and synchronous firing activity in solitary microcultures of cortical neurons on chemically patterned multielectrode arrays. In: Offenhäusser A, Rinaldi R (eds) Nanobioelectronics - for Electronics, Biology, and Medicine. Springer, New York, pp 261–275

Salganicoff M, Sarna M, Sax L, Gerstein GL (1988) Unsupervised waveform classification for multi-neuron recordings: a real-time, software-based system. I. Algorithms and implementation. J Neurosci Methods 25:181–187

Sarna MF, Gochin P, Kaltenbach J, Salganicoff M, Gerstein GL (1988) Unsupervised waveform classification for multi-neuron recordings: a real-time, software-based system. II. Performance comparison to other sorters. J Neurosci Methods 25:189–196

Schatzthauer R, Fromherz P (1998) Neuron-silicon junction with voltage-gated ionic currents. Eur J Neurosci 10:1956–1962

Stett A, Egert U, Guenther E, Hofmann F, Meyer T, Nisch W, Haemmerle H (2003) Biological application of microelectrode arrays in drug discovery and basic research. Anal Bioanal Chem 377:486–495

Thomas CA, Springer PA, Loeb GE, Berwald-Netter Y, Okun LM (1972) A miniature microelectrode array to monitor the bioelectric activity of cultured cells. Exp Cell Res 74:61–66

Yeung CK, Ingebrandt S, Krause M, Offenhдusser A, Knoll W (2001) Validation of the use of field effect transistors for extracellular signal recording in pharmacological bioassays. J Pharmacol Toxicol Methods 45:207–214